American Mineralogist, Volume 64, pages 337–351, 1979

High-temperature crystal chemistry of hydrous Mg- and Fe-cordierites

MICHAEL F. HOCHELLA, JR.[1]

Department of Geological Sciences
Virginia Polytechnic Institute and State University
Blacksburg, Virginia 24061

GORDON E. BROWN, JR.

Department of Geology
Stanford University
Stanford, California 94305

FRED K. ROSS AND G. V. GIBBS

Departments of Chemistry and Geological Sciences
Virginia Polytechnic Institute and State University
Blacksburg, Virginia 24061

Abstract

Structural refinements have been completed for a Mg-rich cordierite using data recorded at 24°, 375°, 775° and 24°C (after heating to 775°) and for an Fe-rich cordierite at 24° and 375°C. The mean T–O bond lengths in both cordierites remain unchanged but the mean octahedral bonds (M–O) lengthen upon heating. The unusually low thermal expansion of the Mg-cordierite is the result of its relatively "rigid" tetrahedral framework and the anisotropic expansion of octahedra isolated from each other. This anisotropic expansion leads to a slight rotation of the six-membered rings, a concomitant collapse of the structure parallel to *c*, and an expansion parallel to *a* and *b*. In the Fe-cordierite, the octahedron is more flattened, resulting in *c* being smaller and *a* and *b* being larger than the cell dimensions of the Mg-cordierite. Upon heating Fe-cordierite, there is no evidence for a rotation of the rings, and *a*, *b*, and *c* increase as the M–O bonds expand.

X-ray $\Delta\rho$ maps calculated for the Mg-cordierite showed approximate positions and relative amounts of channel constituents. The peak ascribed to the alkali and other atoms that centers the six-membered rings becomes elongated parallel to *c* upon heating through 375°C. However, the peak ascribed to the oxygen associated with H_2O in the 24° and 375° maps is absent in the 775°C maps. It reappears in maps computed from the 24° (after heating) data. In both cordierites, small amounts of hematite were produced during heating (prematurely halting data collection on the Fe-cordierite), and apparently formed by combination of octahedral and channel iron with oxygen from the channel water molecules.

A re-examination of the water orientation in the channels of the Mg-cordierite using neutron and X-ray $\Delta\rho$ maps does not clearly show either type I [H–O–H in the (100) plane with the H–H vector parallel to *c*] or type II [H–O–H in the (100) plane with the H–H vector parallel to *b*] water, as previously suggested by spectroscopic studies. Instead, our $\Delta\rho$ maps indicate that the water molecule lies in a plane tilted ~29° from (100) and that the H–H vector is tilted ~19° from *c*.

Introduction

Cordierite, $(Mg,Fe)_2Al_4Si_5O_{18}\cdot nH_2O$, has attracted the interest of mineralogists and ceramists because of its widespread formation in moderate- to high-grade metamorphic rocks, its occurrence in a variety of structural states involving different degrees of Al/Si ordering, and its unusually low thermal expansion. Ceramists have found a number of applications for Mg-cordierite as a thermal shock resistant material.

[1] Present address: Department of Geology, Stanford University, Stanford, California 94305.

0003–004X/79/0304–0337$02.00

Among these are use as an insulator for spark plugs, as a refractory coating on metals for internal combustion engines, in the production of dolomitic types of refractories and low-expansion concrete, and as a catalytic support for the treatment of waste gas and automobile exhaust emissions. Perhaps its most important application in the future will be in the fabrication of turbine engines (Gostelow and Restall, 1972). Fe-rich cordierite has been produced in industry but only as a by-product in blast-furnace linings (Richardson, 1949), in "black cores" in stoneware pipe (Lach, 1974), and even in building-brick (Rathgeber and Fowler, 1966). Because it is more difficult to synthesize than Mg-cordierite and because it oxidizes at high temperatures, ceramists have not yet found specific applications for Fe-rich cordierite.

Despite the extensive use of Mg-cordierite in the ceramic industry and the growing geologic importance of both the Mg- and Fe-rich phases (see, *e.g.*, Currie, 1971; Newton, 1972), no detailed study of the behavior of the cordierite structure at high temperatures has been undertaken. The present study (see Hochella, 1977) was carried out in order to determine the crystal structures of hydrous Mg- and Fe-rich cordierite as a function of temperature, in an attempt to clarify the unusual thermal-expansion properties of this mineral. Also, the effects of heating on both the channel constituents and the Al/Si distribution in the tetrahedral framework were investigated. Finally, the neutron diffraction data of Cohen *et al.* (1977) for the White Well cordierite were re-analyzed, and the orientation of the water molecules within the channels of this structure is discussed.

Experimental detail and observations

Specimen descriptions

The Mg-rich cordierite, designated the White Well cordierite, was previously described and used in a combined X-ray and neutron diffraction study by Cohen *et al.* (1977). It occurs in a phlogopite schist which formed under amphibolite to granulite facies conditions (Pryce, 1973) and is one of the most Mg-rich specimens yet reported (see Table 1). We assumed that our crystal (0.30 × 0.22 × 0.22 mm) and those used by Cohen *et al.* (1977) had identical chemical compositions and crystal structures because they had statistically-identical cell dimensions and were selected from the same specimen (an approximately 4-mm cube). The room-temperature intensity data (before heating) were taken from Cohen (1975).

The Fe-rich cordierite (Table 1), designated the Dolni Bory cordierite, was collected from a pegmatite near Dolni Bory, Western Moravia, Czechoslovakia (Stanek and Miskovsky, 1964), where crystals are reported to attain dimensions up to several decimeters. Many single crystals were sector-twinned; however, one exhibiting uniform optical extinction was found suitable for structure determination. This crystal was a nearly equant chip measuring 0.33 × 0.33 × 0.27 mm. After orientation by optical spindle-stage techniques (Bloss, in preparation), crystals of the White Well and Dolni Bory cordierites were mounted in high-temperature mullite cement on silica-glass fibers and sealed in evacuated silica-glass capillaries to inhibit the oxidation of iron. Each was heated for approximately 12 hours at 100°C to cure the cement and was then equilibrated for at least 12 hours at the temperature of the measurement before data collection was begun. Temperature fluctuations for the single-crystal heater (see Brown *et al.*, 1973, for details) were recorded continuously on a strip chart during each high-temperature experiment and were not more than ±10°.

Thermal expansion measurements

Cell parameters for the White Well cordierite at seven temperatures ranging from 24° to 775° and again at 24°C after heating (see Table 2) were determined by least-squares refinement of the diffractome-

Table 1. Cell parameters (24°C), distortion index (Δ), specific gravity, calculated density (ρ) and composition of the White Well and Dolni Bory cordierites

	White Well	Dolni Bory
a	17.088 (3)[1] Å	17.230(5) Å
b	9.734(2)	9.835(3)
c	9.359(1)	9.314(3)
Δ	0.25°	0.21°
s.g.	2.57	2.76
ρ (calc.)	2.56 g/cm^3	2.78 g/cm^3
Formulae[2]	(based on 18 oxygens)	
Alkalis	$Na_{0.05}K_{0.02}Ca_{0.02}$	$Na_{0.15}Ca_{0.05}$
M cations	$Mn_{0.01}Mg_{1.91}Fe^{2+}_{0.08}$	$Mn_{0.08}Mg_{0.25}Fe^{2+}_{1.65}$
T cations	$Si_{5.01}Al_{3.95}$	$Si_{4.91}Al_{4.05}$
Water	$(H_2O)_{0.56}$	$(H_2O)_{0.61}$

1 *The number in parentheses represents the standard error (1σ) associated with the last decimal place reported.*

2 *White Well cordierite composition reported by Pryce (1973); Dolni Bory cordierite composition reported by Stanek and Miskovsky (1964).*

Table 2. Cell edges (A), cell volume (A³), and calculated distortion index (Δ) *vs.* temperature for White Well and Dolni Bory cordierites

Temperature (°C)	*a*	*b*	*c*	*V*	Δ
White Well cordierite					
24	17.088(3)[1]	9.734(2)	9.359(1)	1556.7(4)	0.25
280	17.103(3)	9.737(2)	9.357(1)	1558.2(4)	0.26
375	17.113(3)	9.741(1)	9.358(1)	1560.0(3)	0.27
470	17.123(2)	9.745(1)	9.357(1)	1561.3(3)	0.27
590	17.132(2)	9.751(1)	9.357(1)	1563.1(3)	0.27
664	17.140(2)	9.755(1)	9.355(1)	1564.2(3)	0.27
775	17.149(2)	9.759(1)	9.352(1)	1565.1(3)	0.27
24[2]	17.119(2)	9.746(1)	9.361(1)	1561.8(3)	0.26
Dolni Bory cordierite					
24	17.230(5)	9.835(3)	9.314(3)	1578.3(8)	0.21
375	17.258(3)	9.847(2)	9.328(2)	1585.3(3)	0.22

1 *The numbers in parentheses represent the estimated standard error ($1\hat{\sigma}$) of the last decimal quoted*

2 *After heating*

ter settings angles for 28 reflections in the 2θ range 30–40°. Similar refinements were carried out for the Dolni Bory cordierite using data gathered at 24° and 375°C. The refined cell parameters, cell volume, and calculated distortion index (Miyashiro *et al.*, 1955) for each temperature are listed in Table 2.

Data collection and refinements

Intensity data from one octant of the Mo$K\alpha$ sphere were collected over a range of 5° to 60° 2θ at temperatures of 375°, 775°, and 24°C (after heating) using graphite-monochromatized MoK radiation (White Well cordierite) and at 24° and 375°C using Zr-filtered MoK radiation (Dolni Bory cordierite)[2]. The upper 2θ limit was imposed by the heater configuration. Two standard reflections (060 and 008) measured every 30 reflections indicated that machine drift and/or crystal movement were within acceptable limits, so no drift corrections were applied. Observed intensities for the White Well cordierite were corrected for Lorentz-polarization effects assuming a 50 percent ideally mosaic monochromator crystal and were converted to $|F(\text{obs})|$ with σ values estimated using the equation of Corfield *et al.* (1967). The observed intensities for the Dolni Bory cordierite were corrected for Lorentz-polarization effects and converted to $|F(\text{obs})|$ with the program DATALIB[3]. Absorption corrections were not initially applied to either the White Well (μ = 9.0 cm^{-1}) or Dolni Bory (μ = 26.3 cm^{-1}) cordierite data sets for the following reasons: (1) Positional parameters obtained from both X-ray and neutron refinements for the White Well cordierite of Cohen *et al.* (1977) are identical to within $2\hat{\sigma}$; the X-ray data were uncorrected for absorption. (2) The relatively low linear-absorption coefficient and size of the White Well cordierite crystal used in this study result in a differential absorption of about 7 percent in the worst case. (3) The Dolni Bory crystal was dislodged and lost from its mount before its shape was accurately determined. However, the crystal was nearly equant and, in the worst case, produced a difference in transmission of ~16 percent. After completion of this study, an absorption calculation for the White Well cordierite crystal was made using the program AGNOST written by Coppens *et al.* (1965), which showed that transmission varied from 0.84 to 0.90. Thus our neglect of an absorption correction in this case should not result in significant errors in positional parameters. In the case of our Fe-rich cordierite, where absorption is more significant (transmission is predicted to vary between 0.42 and 0.49 in the worst cases), the roughly equant shape of the crystal would result in a differential absorption of 10 percent or less between most pairs of reflections. Furthermore, the bond lengths from the two Fe-cordierite refinements are quite reasonable relative to the Mg-cordierite distances, suggesting that the Fe-cordierite positional parameters were not significantly affected by differential absorption effects.

An approximate extinction correction was made and least-squares refinements were calculated with first isotropic and later anisotropic temperature-factor models. Weights based on the counting statistics were used in all refinements, and reflections were automatically rejected at the $2\hat{\sigma}$ level for the White Well cordierite and at $3\hat{\sigma}$ for the Dolni Bory cordierite. In our refinement of the White Well cordierite, we neglected the channel constituents reported in the chemical analysis (Table 1). On the other hand, while neglecting the water, we included the alkali atoms in our refinement for the Dolni Bory cordierite because of their greater abundance. The number of accepted reflections and the weighted and unweighted R factors for the anisotropic refinements are given for both cordierites in Table 3. The final positional parameters and anisotropic temperature factors, as well as the isotropic equivalent temperature factors for the non-equivalent atoms in the White Well and Dolni Bory cordierites, are listed in Table 4. Observed and calcu-

[2] Intensity data for the White Well cordierite were collected at Stanford University; data for the Dolni Bory cordierite were collected at VPI and SU.

[3] Catalogued in the World List of Crystallography Computer Programs (3rd edition).

Table 3. Results of the anisotropic refinements for the White Well and Dolni Bory cordierites

Cordierite	Temperature	# of accepted reflections	R-factor UNW[1]	R-factor W[2]
White Well	24°C (after Cohen *et al.*, 1977)	1057	0.033	0.051
	375°C	1077	0.041	0.066
	775°C	994	0.056	0.087
	24°C (after heating)	1176	0.038	0.061
Dolni Bory	24°C	1203	0.073	0.063
	375°C	716	0.061	0.063

1 $R(UNW) = \Sigma[|F_o| - |F_c|]/\Sigma|F_o|$

2 $R(W) = [\Sigma w(|F_o| - |F_c|)^2/\Sigma w(F_o)^2]^{\frac{1}{2}}$

lated structure factors are given in Table 5.[4] Selected interatomic distances and angles uncorrected for thermal motion were calculated with the program ORFEE[3] and are given in Table 6.

Precession photographs of the White Well cordierite recorded following the heating experiment showed powder rings of weak intensity identified as the diffraction pattern of hematite. Later, when the Dolni Bory cordierite was heated above 600°C, the crystal changed from colorless to amber while the peak intensities dropped off drastically, preventing the collection of additional data. A second crystal was selected and the measurements were repeated, but again the peak intensities dropped off markedly at temperatures above 600°. Precession photographs recorded after the second set of measurements showed the same faint powder rings of the hematite diffraction pattern. Rathgeber and Fowler (1966) carried out open-air heating experiments at 1150° on stoichiometric Fe-cordierite, in which they noticed a reddening of the crystals, a 40 percent decrease in measured X-ray powder diffraction peak intensity, and the formation of hematite (see also Strunz *et al.*, 1971). On the other hand, hedenbergite, $CaFeSi_2O_6$, was heated without oxidation as high as 1000° for data collection by Cameron *et al.* (1973), using the same heater and mounting techniques employed in our study. Brown and Prewitt (1973) heated an olivine (Fa_{31}) to 710°C in an evacuated capillary with no loss in the intensities of the diffraction data nor evidence of oxidation or breakdown. However, unlike cordierite, both of these minerals lack loosely-bound water molecules and Fe atoms in the channels (Goldman *et al.*, 1977). Upon heating, these components apparently react to produce hematite even in a thoroughly evacuated capillary. The decrease in the intensities of the diffraction data recorded for the Dolni Bory cordierite indicates that octahedral Fe is also involved in the reaction to form hematite, which results in partial disruption of the Fe-cordierite structure.

Discussion

Axial expansion

The *a* cell edge of the White Well cordierite increases as a function of temperature at a rate slightly greater than that of *b*, while *c* undergoes a slight but systematic shortening up to 775°C (Fig. 1). On the other hand, the *c* cell edge of the Dolni Bory cordierite (not plotted) does not shorten upon heating from 24° to 375°C but increases at about the same rate as the *a* and *b* cell dimensions. However, because all parameters of the Dolni Bory cordierite were determined at only two temperatures up to 375°C (Table 2), the variation of these parameters and cell volume with temperature is only qualitatively known over a relatively small temperature range. Therefore, the rates of axial and volume expansion for the two cordierites cannot be quantitatively compared.

Thermal expansion data for the disordered polymorph, indialite[5] (*P6/mcc*), measured by Fischer *et al.* (1974) and by Lee and Pentecost (1976), are compared with those for the ordered White Well cordierite (*Cccm*) in Figure 1. The expansion of the *a* cell edge of White Well cordierite is about 1500ppm greater at 775° than that of indialite, whereas the expansion along *b* in the former is practically the same as that along *a* in the latter. The contraction along *c* in White Well cordierite is significantly less (~800ppm less at 775°) than that along *c* in indialite. Moreover, the variation of *c* in White Well cordierite is linear with temperature within the limits of error of the results. The thermal expansion measurements for the two indialites show an initial contraction along *c* with temperature, but Fischer *et al.* find that *c* begins

[4] To receive a copy of Table 5, order Document AM-79-093 from the Business Office, Mineralogical Society of America, 1909 K Street, N.W., Washington, D.C. 20006. Please remit $1.00 in advance for the microfiche.

[5] Cordierite may exist in a range of structural states, like alkali feldspars, depending on the ordering of Al and Si in the tetrahedral framework. The ordered form of cordierite is orthorhombic; the completely disordered form is hexagonal and has been given the name indialite.

Table 4. Final fractional coordinates and thermal parameters ($\times 10^6$) for White Well and Dolni Bory cordierites at various temperatures

Atom		White Well				Dolni Bory	
		24°C[1]	375°C	775°C	24°C[2]	24°C (*Ccem*)	375°C
	x	1/4	1/4	1/4	1/4	1/4	1/4
	y	1/4	1/4	1/4	1/4	1/4	1/4
	z	0.2502(1)[4]	0.2500(2)	0.2500(2)	0.2502(1)	0.2502(3)	0.2501(4)
	β_{11}	57(3)	93(4)	125(6)	51(3)	41(6)	94(9)
T_1^1(Al)	β_{22}	133(8)	224(12)	363(19)	106(10)	104(15)	208(28)
	β_{33}	110(9)	272(14)	429(22)	174(12)	64(15)	104(26)
	β_{12}	15(3)	22(5)	35(8)	15(4)	14(7)	38(12)
	β_{13}	0	0	0	0	0	0
	β_{23}	0	0	0	0	0	0
	B_{eq}[3]	0.52	0.96	1.46	0.54	0.37	0.80
	x	0	0	0	0	0	0
	y	1/2	1/2	1/2	1/2	1/2	1/2
	z	1/4	1/4	1/4	1/4	1/4	1/4
	β_{11}	39(3)	60(5)	88(7)	33(4)	31(8)	17(10)
T_1^6(Si)	β_{22}	146(10)	245(15)	352(22)	170(12)	122(20)	219(34)
	β_{33}	98(10)	228(17)	342(25)	135(15)	44(20)	144(35)
	β_{12}	0	0	0	0	0	0
	β_{13}	0	0	0	0	0	0
	β_{23}	0	0	0	0	0	0
	B_{eq}	0.45	0.81	1.19	0.50	0.33	0.52
	x	0.1926(1)	0.1920(1)	0.1917(1)	0.1924(1)	0.1901(1)	0.1894(2)
	y	0.0778(1)	0.0783(1)	0.0785(2)	0.0778(1)	0.0794(2)	0.0795(3)
	z	0	0	0	0	0	0
	β_{11}	38(2)	60(4)	87(5)	32(3)	37(6)	65(9)
T_2^1(Si)	β_{22}	83(7)	155(11)	240(15)	91(9)	38(14)	144(25)
	β_{33}	118(8)	239(11)	373(20)	167(12)	64(17)	117(29)
	β_{12}	7(3)	11(5)	13(7)	1(4)	12(7)	4(12)
	β_{13}	0	0	0	0	0	0
	β_{23}	0	0	0	0	0	0
	B_{eq}	0.39	0.71	1.08	0.44	0.31	0.58
	x	0.0508(1)	0.0506(1)	0.0500(1)	0.0508(1)	0.0501(1)	0.0499(2)
	y	0.3079(1)	0.3076(1)	0.3070(2)	0.3079(1)	0.3076(2)	0.3077(3)
	z	0	0	0	0	0	0
	β_{11}	31(3)	62(4)	91(6)	32(3)	33(7)	43(9)
T_2^6(Al)	β_{22}	121(8)	220(12)	335(18)	124(10)	64(16)	162(28)
	β_{33}	132(9)	268(15)	382(22)	153(13)	69(19)	208(32)
	β_{12}	8(3)	21(5)	27(8)	5(4)	13(8)	39(13)
	β_{13}	0	0	0	0	0	0
	β_{23}	0	0	0	0	0	0
	B_{eq}	0.43	0.83	1.23	0.46	0.29	0.62
	x	-0.1352(1)	-0.1351(1)	-0.1347(1)	-0.1352(1)	-0.1347(1)	-0.1350(2)
	y	0.2375(1)	0.2369(1)	0.2363(2)	0.2374(1)	0.2343(2)	0.2344(3)
	z	0	0	0	0	0	0
	β_{11}	37(2)	57(4)	86(5)	23(3)	34(7)	59(9)
T_2^3(Si)	β_{22}	99(7)	176(11)	273(16)	133(9)	43(15)	151(26)
	β_{33}	105(8)	247(13)	340(19)	141(11)	73(16)	140(28)
	β_{12}	-11(3)	-14(4)	-40(7)	-13(4)	-22(7)	-12(12)
	β_{13}	0	0	0	0	0	0
	β_{23}	0	0	0	0	0	0
	B_{eq}	0.39	0.73	1.08	0.44	0.28	0.59
	x	0.2474(1)	0.2470(1)	0.2468(2)	0.2473(1)	0.2442(2)	0.2438(3)
	y	0.1029(1)	0.1036(2)	0.1042(3)	0.1034(2)	0.1052(3)	0.1049(5)
	z	0.1410(2)	0.1407(3)	0.1398(4)	0.1409(2)	0.1415(3)	0.1412(5)
	β_{11}	74(5)	137(7)	217(12)	66(5)	69(12)	101(16)
O_1^1	β_{22}	153(13)	277(22)	414(36)	282(16)	129(27)	296(52)
	β_{33}	179(15)	308(25)	450(38)	153(20)	93(28)	269(56)
	β_{12}	9(5)	24(9)	16(16)	3(8)	-15(14)	18(23)
	β_{13}	-31(6)	-40(11)	-122(19)	-31(8)	-44(16)	-80(26)
	β_{23}	-19(11)	-68(19)	-95(29)	-11(16)	-34(24)	-40(44)
	B_{eq}	0.69	1.25	1.90	0.79	0.55	1.10
	x	0.0620(1)	0.0620(1)	0.0619(2)	0.0623(1)	0.0611(2)	0.0609(3)
	y	0.4160(2)	0.4166(2)	0.4159(3)	0.4166(2)	0.4144(4)	0.4151(5)
	z	0.1512(2)	0.1512(3)	0.1510(4)	0.1513(2)	0.1522(4)	0.1509(5)
	β_{11}	54(5)	90(7)	122(10)	57(5)	70(12)	95(15)
O_1^6	β_{22}	211(13)	376(21)	550(33)	215(17)	207(29)	324(48)
	β_{33}	180(15)	331(25)	545(39)	198(21)	134(33)	285(60)
	β_{12}	17(6)	24(10)	23(16)	-3(8)	30(14)	23(23)
	β_{13}	-2(6)	-16(11)	-73(17)	10(8)	23(16)	-18(25)
	β_{23}	-71(11)	-150(19)	-234(32)	-72(15)	-58(26)	-131(46)
	B_{eq}	0.69	1.21	1.81	0.73	0.69	1.13

Table 4. (continued)

		White Well				Dolni Bory	
Atom		24°C[1]	375°C	775°C	24°C[2]	24°C (*Cccm*)	375°C
	x	-0.1732(1)	-0.1736(1)	-0.1734(2)	-0.1733(1)	-0.1729(2)	-0.1729(3)
	y	0.3101(2)	0.3090(2)	0.3082(4)	0.3102(2)	0.3053(4)	0.3049(5)
	z	0.1416(2)	0.1418(3)	0.1422(4)	0.1414(2)	0.1428(4)	0.1427(5)
	β_{11}	54(4)	111(7)	179(12)	60(5)	80(13)	65(17)
O_1^3	β_{22}	202(14)	342(22)	501(35)	174(17)	186(30)	454(56)
	β_{33}	199(15)	285(25)	549(42)	209(21)	94(30)	254(60)
	β_{12}	-11(6)	-26(10)	-55(17)	-20(8)	-21(14)	-45(23)
	β_{13}	20(6)	36(10)	95(18)	21(8)	3(15)	46(22)
	β_{23}	-29(11)	-90(19)	-140(32)	-39(15)	-84(25)	-25(49)
	B_{eq}	0.70	1.20	1.98	0.70	0.67	1.14
	x	0.1223(1)	0.1220(2)	0.1216(3)	0.1222(2)	0.1188(3)	0.1200(5)
	y	0.1839(2)	0.1846(4)	0.1843(6)	0.1844(3)	0.1822(6)	0.1833(8)
	z	0	0	0	0	0	0
	β_{11}	70(7)	135(12)	165(18)	73(8)	72(20)	137(27)
O_2^1	β_{22}	248(21)	368(35)	615(59)	178(25)	176(45)	270(78)
	β_{33}	386(25)	718(50)	1206(94)	401(36)	404(64)	702(109)
	β_{12}	51(9)	133(16)	217(27)	61(12)	66(20)	109(38)
	β_{13}	0	0	0	0	0	0
	β_{23}	0	0	0	0	0	0
	B_{eq}	1.04	1.83	2.83	0.98	0.97	1.71
	x	-0.0430(1)	-0.0434(2)	-0.0438(3)	-0.0432(2)	-0.0435(4)	-0.0434(4)
	y	0.2476(2)	0.2478(4)	0.2484(6)	0.2487(3)	0.2449(6)	0.2462(9)
	z	0	0	0	0	0	0
	β_{11}	53(7)	69(11)	122(17)	58(8)	40(20)	56(25)
O_2^6	β_{22}	301(21)	594(39)	883(69)	261(25)	363(56)	579(94)
	β_{33}	330(24)	711(49)	875(76)	360(34)	494(66)	607(101)
	β_{12}	-27(9)	-31(15)	-14(26)	-33(12)	-16(25)	-107(38)
	β_{13}	0	0	0	0	0	0
	β_{23}	0	0	0	0	0	0
	B_{eq}	0.97	1.85	2.62	0.98	1.20	1.67
	x	-0.1645(1)	-0.1641(2)	-0.1630(3)	-0.1646(2)	-0.1615(4)	-0.1607(7)
	y	0.0792(2)	0.0793(3)	0.0778(5)	0.0803(3)	0.0778(5)	0.0766(7)
	z	0	0	0	0	0	0
	β_{11}	91(7)	163(12)	243(20)	88(8)	90(19)	190(29)
O_2^3	β_{22}	144(19)	189(30)	298(45)	140(25)	101(40)	115(70)
	β_{33}	361(23)	779(50)	850(70)	412(35)	382(59)	621(104)
	β_{12}	-37(9)	-76(15)	-155(25)	-2(12)	7(22)	-69(35)
	β_{13}	0	0	0	0	0	0
	β_{23}	0	0	0	0	0	0
	B_{eq}	0.96	1.79	2.32	1.00	0.93	1.62
	x	0.1625(1)	0.1622(1)	0.1626(1)	0.1624(1)	0.1632(1)	0.1632(1)
	y	1/2	1/2	1/2	1/2	1/2	1/2
	z	1/4	1/4	1/4	1/4	1/4	1/4
	β_{11}	48(3)	75(4)	109(7)	44(3)	47(4)	80(5)
M	β_{22}	142(9)	259(14)	385(20)	122(11)	119(8)	256(15)
	β_{33}	181(9)	436(16)	655(26)	225(13)	162(9)	402(18)
	β_{12}	0	0	0	0	0	0
	β_{13}	0	0	0	0	0	0
	β_{23}	0(7)	8(12)	30(20)	5(10)	12(10)	11(17)
	B_{eq}	0.58	1.13	1.68	0.59	0.53	1.11

[1] *All 24°C data from Cohen et al. (1977)*

[2] *After heating*

[3] *B_{eq} is the isotropic equivalent of the anisotropic temperature factors calculated using the expression (Hamilton, 1959)*

$$B_{eq} = 4/3\ [\beta_{11}a^2 + \beta_{22}b^2 + \beta_{33}c^2 + 2\beta_{12}abcos\gamma + 2\beta_{23}bccos\alpha + 2\beta_{13}accos\beta]$$

[4] *The numbers in parenthesis refer to the estimated standard error ($1\hat{\sigma}$) associated with the last decimal place reported.*

Table 6. T–O and M–O interatomic distances (A) and O–T–O angles (°) for the five tetrahedral sites *vs.* temperature in White Well and Dolni Bory cordierites

Distance/ Angle	Multi- plicity	White Well					Dolni Bory	
		24°C	375°C	775°C	775°C[1]	24°C[2]	24°C	375°C
$T_1 1$–$O_1 1$	[2]	1.760(2)	1.756(2)	1.758(3)	1.755	1.758(2)	1.748(4)	1.756(5)
–$O_1 3'$	[2]	1.757(2)	1.751(2)	1.751(3)	1.762	1.761(2)	1.748(4)	1.750(5)
Mean		1.758(1)	1.753(1)	1.754(2)	1.759	1.759(1)	1.748(2)	1.753(3)
$O_1 3''$–$T_1 1$–$O_1 3'$	[1]	109.6(1)	109.3(2)	109.6(3)	109.0	109.6(1)	110.4(3)	110.3(4)
$O_1 1$–$T_1 1$–$O_1 3''$	[2]	94.7(1)	95.3(1)	95.6(2)	95.3	94.8(1)	96.9(2)	97.2(2)
–$O_1 3'$	[2]	125.9(1)	124.6(1)	125.2(2)	125.4	125.9(1)	122.7(2)	122.4(2)
–$O_1 1'$	[1]	109.0(1)	108.7(2)	180.2(2)	109.3	108.8(2)	109.3(2)	109.3(4)
Mean		110.0(1)	110.0(1)	109.9(1)	109.9	110.0(1)	109.8(1)	109.8(1)
$T_1 6$–$O_1 6$	[4]	1.626(2)	1.625(2)	1.631(3)	1.626	1.628(2)	1.627(4)	1.631(5)
Mean		1.626(2)	1.625(2)	1.631(3)	1.626	1.628(2)	1.627(2)	1.631(3)
$O_1 6$–$T_1 6$–$O_1 6'$	[2]	119.7(1)	120.0(2)	119.6(3)	119.5	120.0(1)	117.6(3)	118.3(4)
–$O_1 6'''$	[2]	110.7(1)	110.6(2)	110.7(3)	110.8	110.8(1)	111.9(3)	110.9(4)
–$O_1 6''$	[2]	98.7(1)	98.5(2)	98.7(2)	98.8	98.2(1)	99.3(3)	99.7(3)
Mean		109.7(1)	109.7(1)	109.7(1)	107.7	109.7(1)	109.6(1)	109.6(2)
$T_2 1$–$O_1 1$	[2]	1.636(2)	1.638(3)	1.633(3)	1.637	1.638(2)	1.634(4)	1.636(5)
–$O_2 3'$	[1]	1.601(2)	1.607(3)	1.603(5)	1.602	1.613(3)	1.623(6)	1.616(7)
–$O_2 1$	[1]	1.583(2)	1.584(3)	1.585(5)	1.584	1.589(3)	1.591(5)	1.576(7)
Mean		1.614(1)	1.617(2)	1.614(2)	1.615	1.619(1)	1.621(3)	1.616(3)
$O_1 1$–$T_2 1$–$O_1 1m$	[1]	107.4(1)	107.0(2)	106.4(3)	106.6	107.3(1)	107.6(3)	107.2(4)
–$O_2 1$	[2]	109.7(1)	109.7(1)	109.8(2)	109.9	109.5(1)	110.0(2)	109.7(3)
–$O_2 3'$	[2]	108.3(1)	108.4(1)	108.9(2)	108.5	108.3(1)	108.7(2)	108.7(3)
$O_2 1$–$T_2 1$–$O_2 3'$	[1]	113.3(1)	113.3(1)	113.2(2)	113.3	113.6(1)	111.8(3)	112.5(4)
Mean		109.4(1)	109.4(1)	109.5(1)	109.5	109.4(1)	109.5(1)	109.4(2)
$T_2 3$–$O_1 3$	[2]	1.634(2)	1.640(3)	1.644(4)	1.638	1.637(2)	1.641(3)	1.638(5)
–$O_2 3$	[1]	1.619(2)	1.614(3)	1.622(5)	1.620	1.613(3)	1.607(6)	1.615(7)
–$O_2 6$	[1]	1.578(2)	1.574(3)	1.563(5)	1.580	1.577(3)	1.575(6)	1.586(7)
Mean		1.617(1)	1.617(2)	1.618(2)	1.619	1.616(1)	1.616(2)	1.619(3)
$O_1 3$–$T_2 3$–$O_1 3m$	[1]	108.2(1)	108.0(2)	108.0(3)	107.9	107.9(2)	108.3(3)	108.8(4)
–$O_2 6$	[2]	111.6(1)	111.8(1)	111.8(2)	111.7	111.6(1)	111.9(2)	111.5(3)
–$O_2 3$	[2]	106.8(1)	106.5(1)	106.6(2)	106.8	106.7(1)	107.0(2)	107.4(3)
$O_2 6$–$T_2 3$–$O_2 3$	[1]	111.5(1)	111.8(1)	111.7(1)	111.6	111.6(1)	110.5(3)	110.2(5)
Mean		109.4(1)	109.4(1)	109.4(1)	109.4	109.4(1)	109.4(1)	109.5(2)
$T_2 6$–$O_1 6$	[2]	1.773(2)	1.779(3)	1.779(4)	1.775	1.779(2)	1.773(4)	1.771(5)
–$O_2 1$	[1]	1.716(2)	1.711(3)	1.715(5)	1.717	1.715(3)	1.711(6)	1.721(7)
–$O_2 6$	[1]	1.706(2)	1.710(3)	1.707(5)	1.707	1.710(3)	1.726(6)	1.721(7)
Mean		1.742(1)	1.745(1)	1.746(2)	1.744	1.746(1)	1.746(3)	1.746(3)
$O_1 6$–$T_2 6$–$O_1 6m$	[1]	105.8(1)	105.3(2)	105.0(3)	105.6	105.5(1)	105.9(3)	105.3(4)
–$O_2 6$	[2]	107.8(1)	107.8(1)	108.0(2)	107.8	107.7(1)	108.2(2)	108.1(3)
–$O_2 1$	[2]	109.9(1)	109.8(1)	109.6(2)	109.8	109.8(1)	110.6(2)	110.5(2)
$O_2 1$–$T_2 6$–$O_2 6$	[1]	115.2(1)	115.7(1)	116.1(1)	115.5	115.7(1)	112.9(3)	114.0(4)
Mean		109.4(1)	109.4(1)	109.4(1)	109.4	109.4(1)	109.4(1)	109.4(1)
$T_2 1$–$O_2 1$–$T_2 6$	[2]	176.0(2)	176.3(3)	176.3(4)	176.3	176.3(2)	173.3(4)	175.1(6)
$T_2 1$–$O_2 3$–$T_2 3$	[2]	179.5(2)	179.0(3)	179.5(4)	180.0	179.0(2)	179.0(4)	178.0(6)
$T_2 3$–$O_2 6$–$T_2 6$	[2]	163.5(2)	164.3(3)	164.8(4)	164.0	164.3(2)	162.9(4)	163.6(6)
Mean		173.0(1)	173.2(1)	173.5(2)	173.4	173.2(1)	171.7(2)	172.2(3)

Table 6. (continued)

Distance/ Angle	Multi- plicity	White Well					Dolni Bory	
		24°C	375°C	775°C	775°C[1]	24°C[2]	24°C	375°C
$T_2 1$-$O_1 1$-$T_1 1$	[2]	127.2(1)	127.2(1)	127.7(2)	127.1	127.4(1)	128.7(2)	128.7(3)
$T_2 6$-$O_1 6$-$T_1 6$	[2]	132.9(1)	132.8(1)	132.6(2)	132.9	132.6(1)	133.2(2)	133.4(3)
$T_2 3$-$O_1 3$-$T_1 1$	[2]	128.2(1)	128.7(1)	129.1(2)	128.9	128.3(1)	129.4(2)	129.5(3)
Mean		129.4(1)	129.6(1)	129.8(1)	129.6	129.4(1)	130.4(1)	130.5(1)
$T_1 1$-$O_1 1$-M	[2]	94.9(1)	94.8(1)	94.6(2)	94.9	95.0(1)	94.4(2)	94.1(2)
$T_1 1$-$O_1 3$-M	[2]	94.6(1)	94.6(1)	94.5(2)	94.3	94.6(1)	94.1(2)	93.9(2)
$T_1 6$-$O_1 6$-M	[2]	95.0(1)	95.1(1)	95.0(2)	95.0	95.2(1)	94.1(2)	94.9(2)
$T_2 1$-$O_1 1$-M	[2]	137.7(1)	137.6(1)	137.6(2)	137.8	137.5(1)	136.6(2)	136.9(3)
$T_2 3$-$O_1 3$-M	[2]	137.1(1)	136.3(1)	136.2(2)	136.5	137.0(1)	136.0(2)	136.0(3)
$T_2 6$-$O_1 6$-M	[2]	131.9(1)	131.8(1)	132.0(2)	131.7	131.9(1)	131.1(2)	131.2(3)
Mean		115.3(1)	115.0(1)	115.0(1)	115.0	115.2(1)	114.4(1)	114.5(1)
M_1-$O_1 6$	[2]	2.113(2)	2.111(2)	2.124(4)	2.120	2.110(2)	2.153(4)	2.161(5)
$-O_1 1'$	[2]	2.100(2)	2.116(2)	2.124(4)	2.121	2.110(2)	2.154(4)	2.162(5)
$-O_1 3'$	[2]	2.115(2)	2.127(2)	2.135(4)	2.132	2.119(2)	2.166(3)	2.173(5)
Mean		2.108(1)	2.119(1)	2.128(2)	2.124	2.112(1)	2.158(1)	2.165(3)

[1] *Simulated expansion by DLS. See text.*

[2] *After heating.*

to expand at temperatures greater than 400°, whereas Lee and Pentecost find that c continues to contract at least to 1000°C. However, when Lee and Pentecost annealed their hexagonal specimen to produce an orthorhombic polymorph (with a greater degree of Al/Si order), they discovered that the contraction along c was increased over that of the hexagonal polymorph. Because the degree of Al/Si ordering in indialite is probably variable (Meagher and Gibbs, 1977), and because the contraction properties in the c direction apparently depend on thermal history, structural state, and channel constituents, we believe that the differences in the curves determined by Fischer *et al.* and Lee and Pentecost are real and represent measurements on hexagonal polymorphs with different structural states.

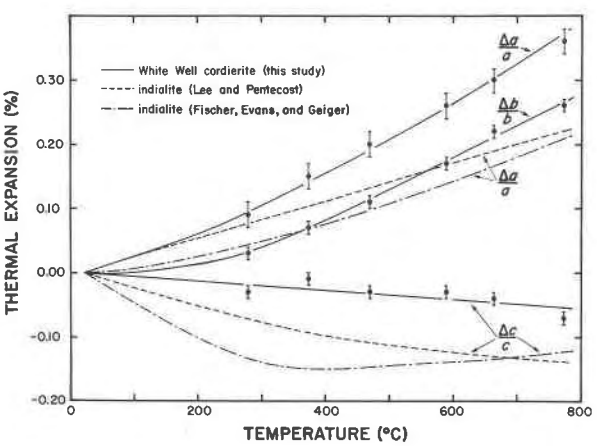

Fig. 1. Axial expansion ($[(X_T - X_{24})/X_{24}] \cdot 100$ where X is a, b or c) *vs.* temperature for two synthetic indialites and the White Well cordierite. The brackets for the White Well data are drawn at $\pm 1\sigma$.

Structure

The crystal structure of cordierite is described by Takane and Takeuchi (1936), Byström (1942), Gibbs (1966), Cohen *et al.* (1977), and Meagher and Gibbs (1977), and consists of a framework of four- and six-membered rings of tetrahedra. The six-membered rings, made up of T_2 tetrahedra, lie in planes perpendicular to c (Fig. 2). The four-membered rings, consisting of alternating T_1 and T_2 tetrahedra, are linked into chains parallelling c which are further crosslinked to form the tetrahedral framework (see Fig. 3). A neutron site refinement by Cohen *et al.* (1977) has shown White Well cordierite to be completely ordered ($t_1 6 = t_2 1 = t_2 3 = 0.0$ and $t_1 1 = t_2 6 = 1.0$ where $t_x y$ represents the probability of finding an Al atom in $T_x y$) within the experimental error. The M atoms (M = Mg,Fe) in cordierite reside within the framework in somewhat flattened octahedra that share two edges with AlO_4 tetrahedra and one with a

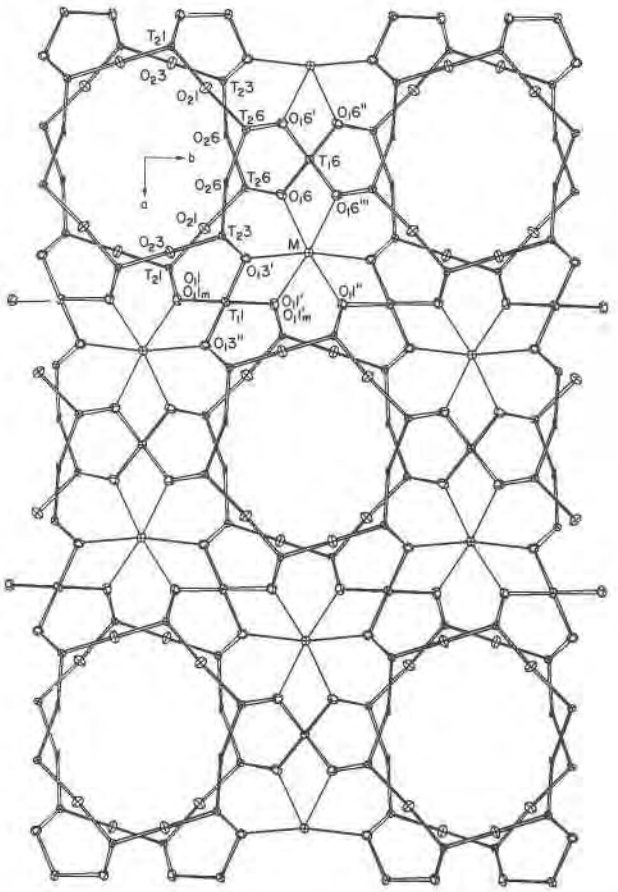

Fig. 2. ORTEP (Johnson, 1965) drawing of the cordierite structure viewed down c (from 0c to ½c). In ordered cordierite, $T_1$1 and $T_2$6 represent Al atoms, while $T_1$6, $T_2$1, and $T_2$3 represent Si atoms. The M octahedra house Mg and Fe.

SiO_4 tetrahedron. The large cavities, connected to form continuous channels parallel to c, house the water molecules in hydrous cordierite. The alkali atoms in alkali-bearing cordierites reside at the centers of the six-membered rings of T_2 tetrahedra (Meagher, 1967).

Isotropic temperature factors

Figure 4a shows the isotropic equivalent temperature factors (B_{eq}) for the cations and oxygens in White Well cordierite plotted against temperature. Si atoms in the six-membered ring have lower temperature factors than Si atoms occupying T_1 tetrahedra or Al atoms occupying T_1 and T_2 tetrahedra; furthermore, the B_{eq} values of the tetrahedrally- coordinated cations increase at the slowest rate relative to other B_{eq} values. The temperature factors for the tetrahedrally-coordinated Al atoms increase slightly faster than for the Si atoms. The M cations show the highest temperature factor and the greatest rate of increase to 775° among cations.

The B_{eq} values for the Dolni Bory cordierite are plotted against temperature in Figure 4b. Despite the limited amount of data, the temperature-factor variation with temperature for each cation has the same general trend as that observed for the White Well cordierite. These observations agree well with findings for the pyroxenes by Cameron *et al.* (1973) and for tremolite by Sueno *et al.* (1973). Both studies show that cations with higher charge and lower coordination have smaller temperature factors that increase more slowly with increasing temperature than cations with lower charge and higher coordination.

The six non-equivalent oxygens in both cordierites are clearly separated into two groups on the basis of B_{eq} values. The three distinct O_1 oxygens are three-coordinated and have smaller temperature factors which increase at a slower rate than those of the three independent O_2 oxygens in the ring which are only two-coordinated. In general, oxygens with high coordination are more restricted in movement and display smaller temperature factors that increase more slowly with increasing temperature than oxygens with lower coordination (*cf.* Burnham, 1964; Sueno *et al.*, 1973).

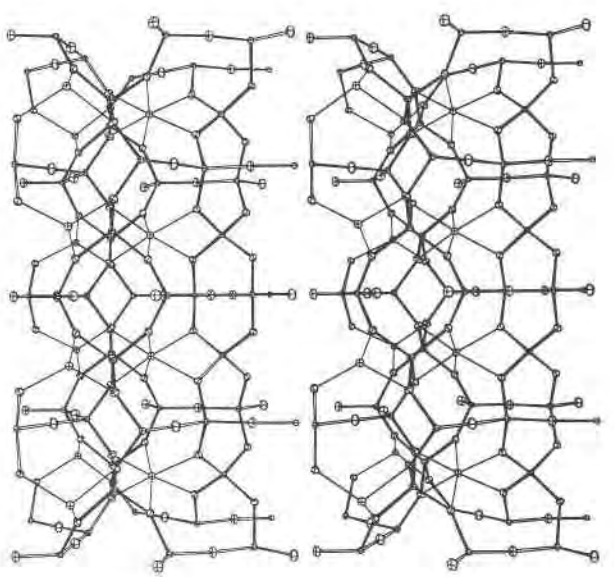

Fig. 3. An ORTEP stereopair drawing showing the four-membered rings which are linked into chains paralleling c. Both symmetrically distinct chains are shown (the two overlying chains on the left are related by a c glide) and have been highlighted by heavy-lined bonds. Note that the octahedron (single line bonds) shares three edges with tetrahedra. In this figure, a is horizontal and c is vertical.

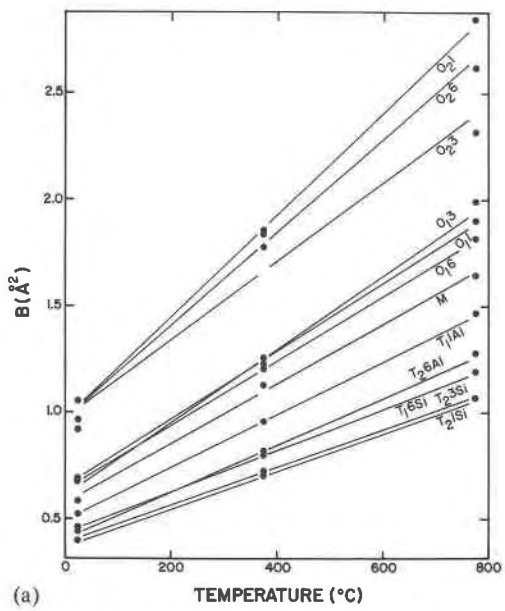

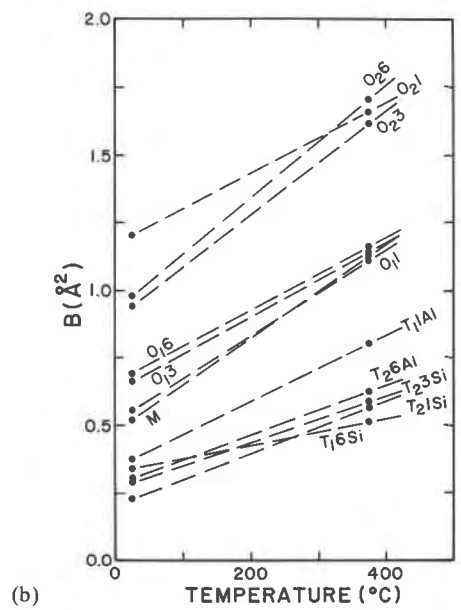

Fig. 4. (a) Isotropic equivalent temperature factors (B_{eq}) for the White Well cordierite plotted as a function of temperature from 24° to 775°C. (b) Isotropic equivalent temperature factors (B_{eq}) for the Dolni Bory cordierite plotted as a function of temperature from 24° to 375°C. (The nomenclature of the atoms from *a* and *b* is the same as that in Fig. 2.)

Tetrahedral and octahedral bond length expansion

Mean T–O bond lengths for individual tetrahedra in both the White Well and the Dolni Bory cordierites do not appear to change significantly with temperature (Table 6). Moreover, because they are unchanged after heating in White Well cordierite, we may conclude that the ordered configuration of Al and Si in the tetrahedral framework of low cordierite was unaffected by our heating experiments. On the other hand, the octahedral M–O bonds show a significant increase in length with increasing temperature. The Mg–O bonds in White Well cordierite increase 0.018A on the average when heated from 24° to 775°C whereas the Fe–O bonds in the Dolni Bory cordierite increase by 0.007A when heated from 24° to 375°. In the temperature range 24° to 375°, the mean Fe–O bond length expansion [~0.007(1)A] is less than the mean Mg–O bond length expansion [~0.011(1)A]. This result agrees with similar results obtained by Cameron *et al.* (1973) and is consistent with the notion that the Fe–O bond is stronger than the Mg–O bond.

Table 7. Polyhedral volumes (A^3) *vs.* temperature for White Well and Dolni Bory cordierites

	White Well				Dolni Bory	
Polyhedra	24°C	375°C	775°C	24°C[1]	24°C	375°C
$T_1$1	2.58	2.57	2.58	2.59	2.61	2.63
$T_1$6	2.14	2.13	2.15	2.13	2.16	2.17
$T_2$1	2.15	2.16	2.15	2.17	2.18	2.17
$T_2$6	2.70	2.72	2.72	2.72	2.73	2.72
$T_2$3	2.16	2.16	2.17	2.16	2.16	2.17
M	11.79	11.91	12.06	11.86	12.42	12.55

1 *After heating.*

Volumes of the AlO_4 and SiO_4 tetrahedra show little or no change with heating (see Table 7). In contrast, the MgO_6 octahedra in the White Well cordierite exhibit a volume increase of $0.27A^3$ when heated from 24° to 775°. Similarly, the FeO_6 octahedra in the Dolni Bory cordierite show a volume increase of $0.13A^3$ when heated to 375°C.

The mean thermal expansion of the octahedron in the Mg-rich cordierite ($12.6 \times 10^{-6}°C^{-1}$) is significantly less than that observed for corresponding octahedra in periclase ($13.9 \times 10^{-6}°C^{-1}$), forsterite ($14.2 \times 10^{-6}°C^{-1}$), and diopside ($14.4 \times 10^{-6}°C^{-1}$) (Hazen and Prewitt, 1977). As indicated earlier, the octahedron in cordierite is isolated from other octahedra and shares three of its edges with tetrahedra. Since the dimensions of these tetrahedra show little or no change with heating, they act as rigid clamps and constrain the octahedron in its expansion upon heating. The octahedra in forsterite and diopside share edges with both tetrahedra and octahedra, whereas those in periclase share edges only with other octa-

hedra. Therefore, the mutual expansion of the octahedra in these structures should not be as restricted as in cordierite. If this is true, the mean thermal expansion of an M-polyhedron depends upon its environment as well as on the strength of the M–O bonds. In fact, when trying to predict the thermal expansion of a crystalline material from its structure at 24°C, as attempted by Khan (1976), it may be inappropriate to assign a fixed rate of expansion to an M–O bond from one structure type to another.

A structural interpretation of the thermal expansion of cordierite

The anisotropic thermal expansion of the unit cell of the White Well cordierite is related to the anisotropic thermal expansion of its Mg-rich octahedron and its accompanying effect on the tetrahedral framework. Changes in the thickness of the octahedron measured along *a* and *b* correlate with changes in the lengths of *a* and *b*, respectively (Fig. 5), whereas the octahedral thickness measured along *c* is unaffected by the temperature change. This anisotropic expansion of the octahedron serves to rotate (~0.2°) the rigid six-membered rings clockwise and counterclockwise in alternate layers perpendicular to *c* (Fig. 6). Figure 6 also shows the displacements accompanying this rotation of each of the tetrahedral cations in the rings. The twisting of the tetrahedral framework attending the rotation is associated with a decrease in selected T–O–M and O–T–O angles, which results in a more efficient packing of the structure and a concomitant contraction of the *c* cell edge (Fig. 7).

A distance least-squares *(DLS)* refinement (Meier and Villiger, 1969) of the White Well cordierite structure was undertaken to learn whether the results of such a regression are consistent with our assertion that the thermal expansion of the octahedron is the driving force behind the thermal expansion of cordierite. The T–O bond lengths, the nearest-neighbor O···O separations, and the unit-cell edges used in the calculation were initialized at the values measured at 24°, and the M–O bond lengths were initialized at the values measured at 775°C. In the refinement, each of the T–O and M–O bonds was assigned a weight of

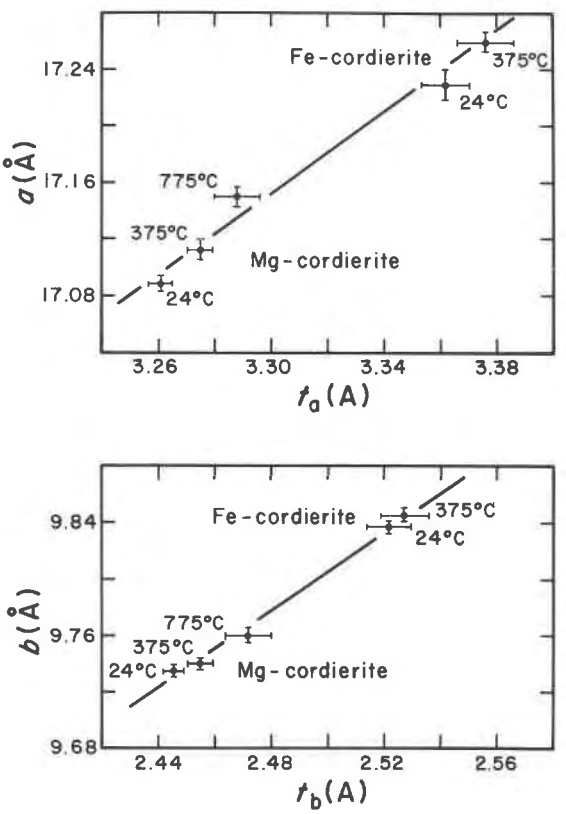

Fig. 5. The *a* and *b* cell edges *vs.* the thickness of the M octahedron measured along a,t_a, and along b,t_b, for the White Well (Mg) and Dolni Bory (Fe) cordierites at various temperatures. The relationships between *a* and t_a and *b* and t_b are similar for both cordierites and seem to be continuous from the Mg- to the Fe-cordierite. The brackets are drawn at $\pm 1\sigma$.

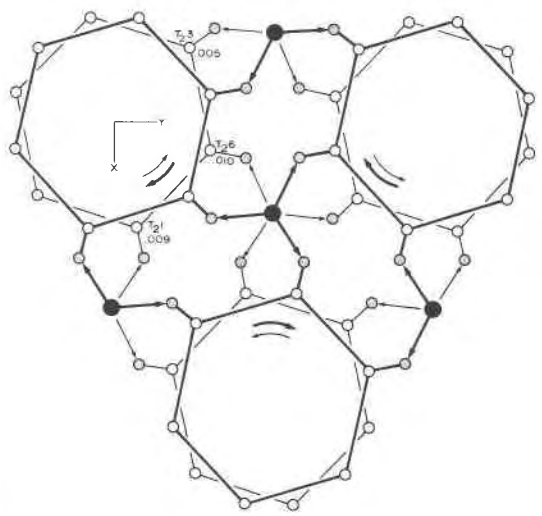

Fig. 6. Rotation of the six-membered rings in the White Well cordierite. The open circles represent the tetrahedral cations in the ring, the dotted circles the O_1 oxygens, and the solid circles the octahedral cations (96 percent Mg). The vectors radiating from the octahedral cation represent the expanding Mg–O bonds. As shown, the upper six-membered rings rotate in a clockwise direction upon heating whereas the lower ones rotate in a counterclockwise direction. The three independent tetrahedral ring sites are labeled together with the distance (in A) that these cations are displaced about the ring over the temperature range 24° to 775°C.

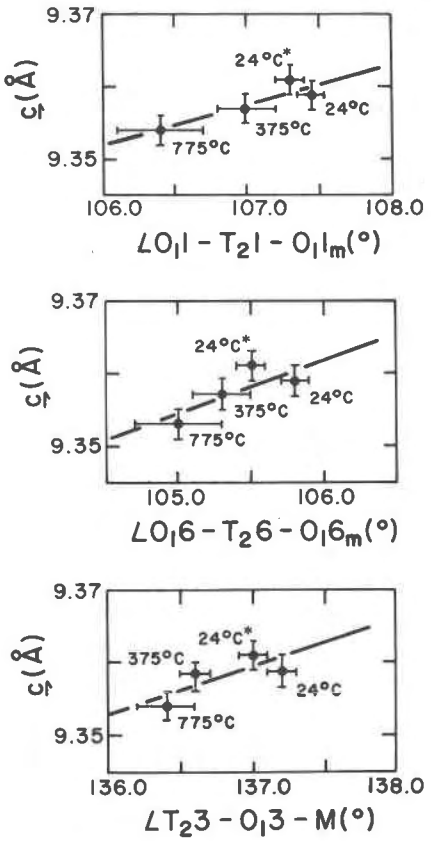

Fig. 7. The length of the *c* cell edge *vs.* one T–O–M and two O–T–O angles at various temperatures for the White Well cordierite. These angles are oriented such that their change directly affects *c*. Their decrease is apparently related to the expansion of the octahedral bonds and slight rotation of the rings. Error bars are drawn at $\pm 1\sigma$. (24°C* is after heating.)

1.0, and each O···O separation was given a weight of 0.25. More than 40 cycles of refinement were calculated in which the positional parameters of the atoms in the asymmetric unit and the cell-edge lengths were simultaneously varied. The resulting cell edges (a = 17.143, b = 9.758, c = 9.348A) agree within about 4 parts in 10,000 with those observed at 775°C [a = 17.149(2), b = 9.759(1), c = 9.352(1)A]. In addition, as the refined T–O and M–O bond lengths are within 0.001A of the starting values, the results of the *DLS* refinement indicate that the anisotropic thermal expansion of the unit cell of cordierite is principally controlled by the thermal expansion properties of the octahedron, as concluded above on the basis of observed structural change with increasing temperature.

As shown in Figure 5, the thickness of the octahedron in the Dolni Bory cordierite measured along *a* and *b* is significantly greater than that measured for the White Well cordierite. This greater thickness conforms with the larger *a* and *b* cell dimensions of the Dolni Bory cordierite. Changes in the thickness of the octahedron measured along *a* and *b* correlate linearly with changes in the cell dimensions of both Dolni Bory and White Well cordierites with increasing temperature (Fig. 5). Despite the larger volume of the Fe-octahedron, the *c* cell dimension of the Dolni Bory cordierite is 0.05A shorter than that measured for the White Well cordierite. However, the thickness of the Fe-rich octahedron along *c* is 0.025A less than that of the Mg-rich octahedron. This difference in octahedral thickness along *c* precisely accounts for the 0.05A difference in the *c* cell dimension between the two cordierites (there are two octahedra along each translational repeat in the *c* direction). Unlike those of the White Well cordierite, both the thickness of the octahedron and the *c* cell dimension of the Dolni Bory cordierite increase with rising temperature. Also, there is no evidence of a rotation of the six-membered rings associated with expansion of the octahedron up to 375°C in the Dolni Bory cordierite.

The effects of heating on channel constituents

The loosely-bound channel constituents in cordierite undergo large anisotropic vibrations and positional changes upon heating, as shown in the $\Delta\rho$ maps at each temperature of refinement for the White Well cordierite (Figs. 8a–d). The peak ascribed to the alkali and Fe atoms at 0,0,0 is elongated parallel to the channel axis, *c*, at 375°, while the Ow (oxygen associated with the water molecule) peak at 0,0,1/4 is a single peak elongated further along *a* than the same peak at 24°C. At 775°C in the White Well cordierite, the Ow peak is absent. It reappears in the 24° (after heating) $\Delta\rho$ map as a single peak, less than half the size of the original Ow peak, and is no longer elongated parallel to *a*. The absence of the peak at 775° is probably due to high-temperature factors and seemingly complete disorder of water molecules within the cavity. The Ow peak also vanishes in the Dolni Bory cordierite in the $\Delta\rho$ map computed from the 375°C data. On the other hand, the peak ascribed to alkali ions centering the six-membered ring has enlarged in the 775°C $\Delta\rho$ map for the White Well cordierite. Also, the 24° (after heating) $\Delta\rho$ map for White Well cordierite shows that there is (1) more electron density at 0,0,0 than in the unheated sample, (2) less electron density at 0,0,1/4, and (3) an overall substantial drop in the original amount of channel constituents. It seems reasonable to suggest that some of the channel constituents have been driven out of the

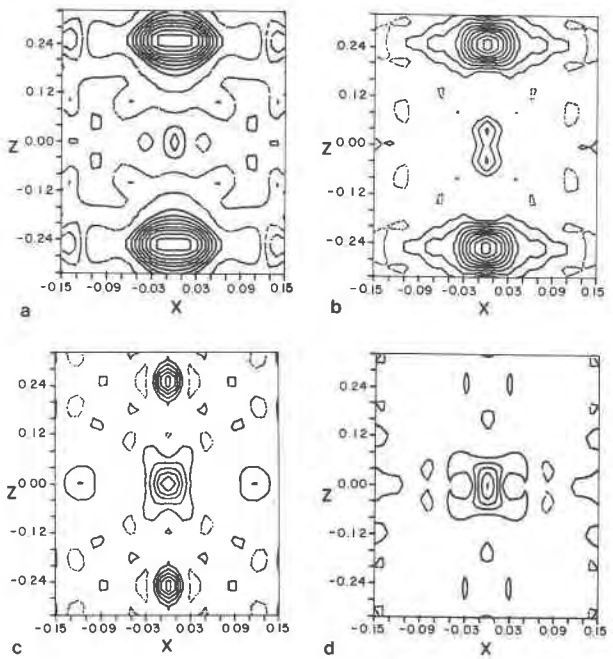

Fig. 8. X-ray $\Delta\rho$ maps of the White Well cordierite showing the peaks ascribed to channel constituents at (a) 24°, (b) 375°, (c) 775°, and (d) 24°C (after heating). All sections are the (010) plane at $y = 0$. Solid contours are positive; dashed contours are negative. The zero contour is omitted, and the contour interval is 0.20e$-$/A^3 for each map.

structure, while some of the remaining H_2O molecules have taken up positions centering the six-membered rings.

The state of the White Well cordierite after heating

The *a* and *b* cell edges of the White Well cordierite do not return to their original lengths after cooling to 24°C (Table 2). Observations such as these are usually attributed to a change in structural state with heating (see, *e.g.*, Karkhanavala and Hummel, 1953; Levien and Papike, 1976). However, this is not the case for the White Well cordierite because its completely ordered structure did not disorder at all during data collection at high temperatures. A possible explanation in this case is that changes in amount and perhaps position of channel constituents with heating and cooling cause *a* and *b* to increase. It is not clear, though, how these changes might affect the $Al_4Si_5O_{18}$ framework, if at all (see Langer and Schreyer, 1976; Stout, 1976). Another more plausible explanation is that some of the iron in the framework was used to form secondary hematite, and as a result some of the octahedra were left empty. Octahedral vacancies take up more space than filled octahedra, and *a* and *b* would be appropriately larger (see Table 7 and Fig. 5). This hypothesis is supported by our observation of powder rings with *d* spacings corresponding to the 104, 110, 024, 116, 214 and 300 spacings of hematite in the precession photographs of heated White Well cordierite. However, if octahedral vacancies existed in the framework after heating, one would expect the isotropic temperature factors of the octahedra to be less after heating than before; this is not the case (Table 4). The observed differences in *a* and *b* dimensions of the White Well cordierite before and after heating are probably due to a combination of the above factors.

Orientation of the water molecules in the White Well cordierite

A re-investigation of the water position in the channels of the White Well cordierite, as located by Cohen *et al.* (1977), has led to a new interpretation of the orientation of water molecules, from the X-ray and neutron diffraction data of Cohen (1975). Although attempts at refining the Ow (oxygen of the water molecule) position during the structure refinement were unsuccessful, X-ray $\Delta\rho$ maps show Ow to be split into two positions along the *x* axis at $\pm 0.027,0,1/4$ as shown in Figure 9. Newly calculated neutron $\Delta\rho$ maps (see Fig. 10) strongly suggest that the plane of the H_2O molecule is inclined by $\sim$29° from (100) and that the H–H vector is 19° from *c*. This H_2O position is significantly different from that proposed by Farrell and Newham (1967) and Tsang and Ghose (1972), based on spectroscopic studies.

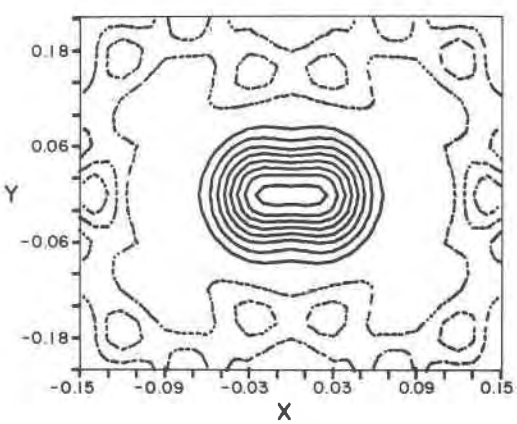

Fig. 9. X-ray $\Delta\rho$ map (24°C) showing the elongated oxygen peak along the *x* axis. Section is the (001) plane at $z = 1/4$. The contour interval is 0.20e$-$/A^3, and the zero contour has been omitted. Solid contours are positive, dashed contours are negative. Subtraction of the peak was most complete when electron density was added at ± 0.027 on *x*.

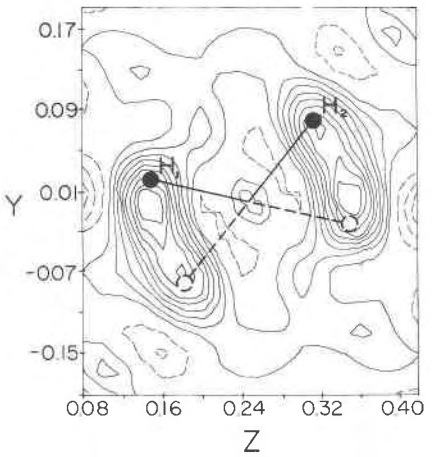

Fig. 10. Neutron $\Delta\rho$ map (24°C) showing the negative scattering of the hydrogens (zero contour omitted) in the (100) plane at x = 0.01. Solid contours are negative, dashed contours are positive. The Ow peak, that ascribed to the oxygen of the water molecule, has been subtracted. The dimensions of the two symmetry-related water molecules shown are d(H1–Ow) = 0.99A, d(H2–Ow) = 1.01A and H1–Ow–H2 = 105.1° with H1 at x = 0.010, y = 0.025, z = 0.150, H2 at x = 0.010, y = 0.078 and z = 0.311 and Ow at x = 0.027, y = 0, z = 1/4.

Their results show the water molecule to be in the (100) plane with the H–H vector parallel to *c*, and we shall refer to water in this proposed orientation as type I after the notation of Wood and Nassau (1967) for water orientation in beryl. Goldman *et al.* (1977) stated that the White Well cordierite, as well as having type I water, has a small amount of type II water [H–O–H in the (100) plane with the H–H vector parallel to *b*], also based on polarized IR spectra. There are two possible hypotheses for explaining the differences between the spectral and crystallographic results: (1) type I and type II water actually exist in the White Well cordierite, and our $\Delta\rho$ maps show the combined scattering of both types, resulting in a space average position, or (2) the actual water position is as shown in our model, and the spectroscopic data show the *b* and *c* components of the true H–H vector. Our data are not consistent with hypothesis (1) and strongly suggest that hypothesis (2) is correct.

Problems arose when we attempted to completely subtract out the Ow peak using the multiplicity of H_2O from the chemical analysis of the White Well cordierite (Pryce, 1973). A negative residual was left at the Ow position on the neutron $\Delta\rho$ map, indicating that the amount of H_2O in the formula is less than $(H_2O)_{0.56}$. A series of calculations with smaller amounts of Ow showed that 0.36 Ow at ±0.027,0,1/4 resulted in a negligible residual in the $\Delta\rho$ map. To further support the idea that less water is present than reported by Pryce (1973), the amount of hydrogen needed to diminish the negative peaks of the neutron $\Delta\rho$ map shown in Figure 10 is consistent with $(H_2O)_{0.36}$. However, a thermal gravimetric weight-loss curve for the White Well cordierite (C. W. Huggins, 1976, personal communication) suggests that the amount of H_2O in the formula is correct.

Acknowledgments

Dr. E. P. Meagher is gratefully acknowledged for performing the *DLS* calculations and for reviewing the manuscript. Dr. P. H. Ribbe also read the manuscript and offered helpful suggestions. Dr. G. R. Rossman is thanked for several helpful discussions on channel constituents in cordierites. We thank Sharon Chiang for drafting the figures and Marie Phillips for her patient typing of the manuscript. This study was supported by NSF grants EAR74-035056-A01 (Brown) and EAR77-23114 (Gibbs and Ribbe).

References

Bloss, F. D. (in preparation) *The Spindle Stage: Principles and Practice.*

Brown, G. E. and C. T. Prewitt (1973) High-temperature crystal chemistry of hortonolite. *Am. Mineral., 58,* 577–587.

———, S. Sueno and C. T. Prewitt (1973) A new single-crystal heater for the precession camera and four-circle diffractometer. *Am. Mineral., 58,* 698–704.

Burnham, C. W. (1964) Temperature parameters of silicate crystal structures. *Am. Mineral., 50,* 282.

Byström, A. (1942) Crystal structure of cordierite. *Arkiv Kemi Mineral. Geol., 15B,* No. 12.

Cameron, M., S. Sueno, C. T. Prewitt and J. J. Papike (1973) High-temperature crystal chemistry of acmite, diopside, hedenbergite, jadeite, spodumene, and ureyite. *Am. Mineral., 58,* 594–618.

Cohen, J. P. (1975) *An X-ray and Neutron Diffraction Study of Hydrous Low Cordierite.* M. S. Thesis, Virginia Polytechnic Institute and State University, Blacksburg, Virginia.

———, F. K. Ross and G. V. Gibbs (1977) An X-ray and neutron diffraction study of hydrous low cordierite. *Am. Mineral., 62,* 67–78.

Coppens, P., L. Leiserowitz and D. Rabinovich (1965) Calculation of absorption correction for camera and diffractometer data. *Acta Crystallogr., 18,* 1035–1038.

Corfield, R., R. J. Doedens and J. A. Ibers (1967) The crystal and molecular structure of nitridodichlorobis(triphenylphosphine)rhenium(V), $ReNCl_2[P(C_6H_5)_3]_2$. *Inorg. Chem., 6,* 197–204.

Currie, K. L. (1971) The reaction 3 cordierite = 2 garnet + 4 sillimanite + 5 quartz as a geological thermometer in the Opinicon Lake region, Ontario. *Contrib. Mineral. Petrol., 33,* 215–226.

Farrell, E. F. and R. E. Newnham (1967) Electronic and vibrational absorption spectra in low cordierite. *Am. Mineral., 52,* 380–388.

Fischer, G. R., D. L. Evans and J. E. Geiger (1974) Crystal lattice thermal expansion of cordierite (abstr.). *Crystallographic Assoc. Progr. and Abstr. Series 2, 2,* 214; and personal communication (1977).

Gibbs, G. V. (1966) The polymorphism of cordierite, I: The crystal

structure of low cordierite. *Am. Mineral., 51,* 1068–1087.

Goldman, D. S., G. R. Rossman and W. A. Dollase (1977) Channel constituents in cordierite. *Am. Mineral., 62,* 1144–1157.

Gostelow, C. R. and J. E. Restall (1972) Ceramic with potential gas turbine application. *Proc. Brit. Ceram. Soc., 22,* 117–127.

Hamilton, W. C. (1959) On the isotropic temperature factor equivalent to a given anisotropic temperature factor. *Acta Crystallogr., 12,* 609–610.

Hazen, R. M. and C. T. Prewitt (1977) Effects of temperature and pressure on interatomic distances in oxygen-based minerals. *Am. Mineral., 62,* 309–315.

Hochella, M. F., Jr. (1977) *High-Temperature Crystal Chemistry of Hydrous Mg- and Fe-rich Cordierites.* M. S. Thesis, Virginia Polytechnic Institute and State University, Blacksburg, Virginia.

Johnson, C. K. (1965) *ORTEP, a Fortran thermal ellipsoid plot program for crystal structure illustrations.* U.S. Tech. Inf. Serv. ORNL 3794.

Karkhanavala, M. D. and F. A. Hummel (1953) The polymorphism of cordierite. *J. Am. Ceram. Soc., 36,* 389–392.

Khan, A. A. (1976) Computer simulation of thermal expansion of non-cubic crystals: forsterite, anhydrite and scheelite. *Acta Crystallogr., A32,* 11–16.

Lach, V. (1974) The occurrence of iron-cordierite in the black cores of stoneware pipes. *Interceram. NR3,* 214–218.

Langer, K. and W. Schreyer (1976) Apparent effects of molecular water on the lattice geometry of cordierite: a discussion. *Am. Mineral., 61,* 1036–1040.

Lee, J. D. and J. L. Pentecost (1976) Properties of flux-grown cordierite single crystals. *J. Am. Ceram. Soc., 59,* 183.

Levien, L. and J. J. Papike (1976) Scapolite crystal chemistry: aluminum–silicon distributions, carbonate group disorder, and thermal expansion. *Am. Mineral., 61,* 864–877.

Meagher, E. P. (1967) *The Crystal Structure and Polymorphism of Cordierite.* Ph.D. Dissertation, The Pennsylvania State University, University Park, Pennsylvania.

——— and G. V. Gibbs (1977) The polymorphism of cordierite. II. The crystal structure of indialite. *Can. Mineral., 15,* 43–49.

Meier, W. M. and H. Villiger (1969) Die Methode der Abstandsverfeinerung zur Bestimmung der Atomkoordinaten idealisierter Gerüststrukturen. *Z. Kristallogr., 129,* 411–423.

Miyashiro, A., T. Iiyama, M. Yamasaki and T. Miyashiro (1955) The polymorphism of cordierite and indialite. *Am. J. Sci., 253,* 185–208.

Newton, R. C. (1972) An experimental determination of the high-pressure stability limits of magnesian cordierite under wet and dry conditions. *J. Geol., 80,* 398–420.

Pryce, M. W. (1973) Low-iron cordierite in phlogopite schist from White Well, Western Australia. *Mineral. Mag., 39,* 241–243.

Rathgeber, R. and H. Fowler (1966) Iron-cordierite in the core structure of a bloated building brick. *J. Aust. Ceram. Soc., 2,* 52–53.

Richardson, H. M. (1949) Occurrence of iron-cordierite in blast furnace linings. *Mineral. Mag., 28,* 547–554.

Stanek, J. and J. Miskovsky (1964) Iron-rich cordierite from a pegmatite near Dolni Bory, W. Moravia, Czechoslovakia. *Casopis Mineral. Geol., 9,* 191–192.

Stout, J. H. (1976) Apparent effects of molecular water on the lattice geometry of cordierite: a reply. *Am. Mineral., 61,* 1041–1044.

Strunz, H., C. H. Tennyson and P. Uebel (1971) Cordierite. *Mineral. Sci. Eng., 3,* 3–18.

Sueno, S., M. Cameron, J. J. Papike and C. T. Prewitt (1973) The high temperature crystal chemistry of tremolite. *Am. Mineral., 58,* 649–664.

Takane, K. and T. Takeuchi (1936) The crystal structure of cordierite. *Japan. Assoc. Mineral. Petrol. Econ. Geol. J., 16,* 101–127.

Tsang, T. and S. Ghose (1972) Nuclear magnetic resonance of ^{1}H and ^{27}Al and Al–Si order in low cordierite, $Mg_2Al_4Si_5O_{18}\cdot nH_2O$. *J. Chem. Phys., 56,* 3329–3332.

Wood, D. L. and K. Nassau (1967) Infrared spectra of foreign molecules in beryl. *J. Chem. Phys., 47,* 2220–2228.

Manuscript received, December 29, 1977;
accepted for publication, September 12, 1978.